# *Contents*

## *Acknowledgements*

This work would not be done without financial support from World Meteorological Organization (WMO). The EMEP/MSC-E gratefully appreciates this assistance.

## *Summary*

This technical note is prepared in the framework of cooperation between World Meteorological Organization (WMO), Arctic Monitoring and Assessment Programme (AMAP), and Meteorological Synthesizing Centre East of Co-operative programme for monitoring and evaluation of the long-range transmission of air pollutants in Europe (EMEP/MSC-E). The objective of the work was to develop and test the atmospheric block of a hemispheric transport model to be used for assessment of atmospheric deposition of persistent organic pollutants (POPs) to the Arctic region as a contribution to the relevant AMAP project.

This note presents results of the development of hemispheric multi-compartment model for HMs and POPs, in particular, its atmospheric block. The model uses horizontal resolution of 2.5º x 2.5º and 10 non-uniform layers in terrain-following coordinates up to the pressure level of 100 hPa in vertical direction. As a part of this activity the system of meteorological data preparation has been developed. This system provides the meteorological information required for modelling of HM and POP long-range transport within the Northern Hemisphere. Several modelling experiments were carried out using the meteorological information and emission data for 1990. Modelling results were compared with available measurements and with results of MSC-E regional POP transport model.

# *Introduction*

In the past few years the efforts of the EMEP/MSC-E have been devoted to the evaluation of long-range transport of heavy metals (HMs) and persistent organic pollutants (POPs) within the European region. However, some of these pollutants, such as, mercury, polychlorinated biphenyls (PCBs), hexachlorocyclohexanes (HCHs), are characterized by rather high volatility and long residence time in the atmosphere. Since 1998 the long-range transport of selected HMs and POPs has been simulated using the regional models developed at the EMEP/MSC-E. The results obtained indicate that essential amounts of volatile pollutants are transported outside the modelling domain. Additional limitation of regional models for mercury and some POPs is connected with the fact that the transport from emission sources located outside the model domain is not taken into account in a proper way. Application of hemispheric multi-compartment model in combination with regional modelling could solve these problems.

Hemispheric modelling can be used for the assessment of contamination of remote regions (such as the Arctic) by different HMs and POPs from emission sources spread over the Northern Hemisphere.

Following the recommendations of the Steering Body to EMEP and the Geneva workshop held in November 1999 [*WMO/GAW No.136*, 2000] MSC-E initiated the development of hemispheric multi-compartment long-range transport model for selected HMs and POPs. This work was supported by WMO in the framework of cooperation between WMO, EMEP, and AMAP. The first stage was devoted to the development of the meteorological data preparation system for the Northern Hemisphere, preparation of meteorological information for modelling, and development of atmospheric part of the model. This technical note includes the description of a hemispheric model, system of meteorological data supply and preliminary modelling results.

At the present stage we focus on the model development and computation experiments for POPs. Similar work for HMs and especially for mercury is planned to be performed in near future. However, the atmospheric part of the model described here is applicable both to POP and HM transport models.

# 1. *Description of the Hemispheric Multi-Compartment Model*

The model presented in this report is a hemispheric multi-compartment model based on a three-dimensional Eulerian atmospheric transport scheme [*Pekar*, 1996; *Pekar et al*., 1998,1999]. This model aimed at evaluating of the long range transport of selected Heavy Metals (HMs) and Persistent Organic Pollutants (POPs), in particular, at first stage mercury, PCBs, HCHs. The modelling domain covers the whole Northern Hemisphere with the horizontal resolution of 2.5ºx2.5º. In vertical direction the terrain following coordinates are used with 10 non-uniform layers up to 100 hPa or approximately 15 km. Figure 1.1 shows the simplified scheme of the model structure.

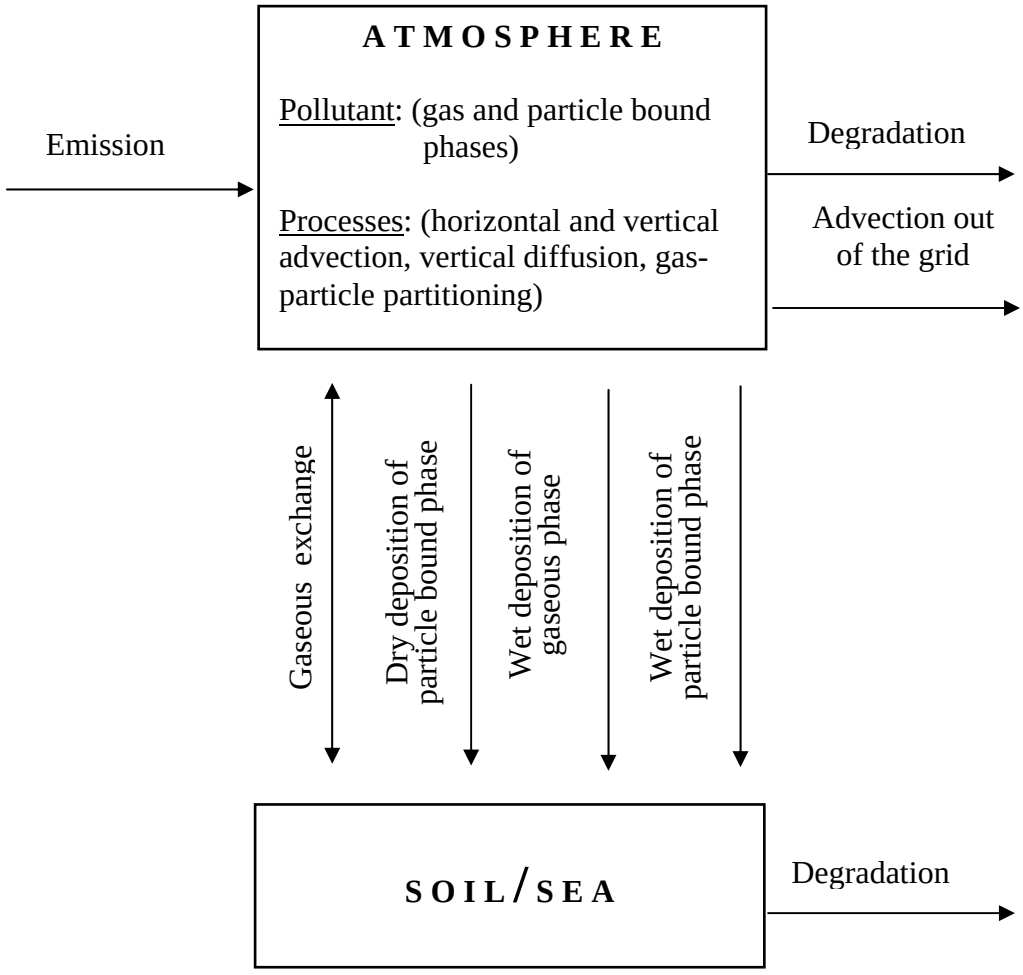


**Figure 1.1.** Simplified scheme of the model

As it can be seen from the Figure 1.1 the following processes are included into the model:

- Pollutant emission to the atmosphere. The total annual emission field is used in the model. The function of the annual emission trend is applied to take into account seasonal variations of emission during a year.
- Horizontal and vertical advection in the atmosphere (including the gaseous and particulate phase of a pollutant).
- Vertical diffusion in the atmosphere (including the gaseous and particulate phase of a pollutant).
- Degradation of a pollutant in the atmosphere, soil and sea water.
- Gaseous exchange between the atmosphere and underlying surface, including soil and sea water.
- Dry deposition of the particulate phase of a pollutant to the land and sea surfaces.
- Wet deposition of the gaseous and particulate phase of a pollutant to the underlying surface.
- Gas-particle partitioning in air.

At the next stages of the model development it is planned to add a description of air-vegetation exchange process and transport with sea currents along with processes occurred with pollutants within the marine environment (sedimentation and partitioning within the water column). For mercury modelling different mercury chemical forms along with equations describing their chemical transformations are to be involved into the model.

## 1.1. *General description of the model*

Three-dimensional equation describing atmospheric advection and turbulent diffusion of a pollutant in spherical co-ordinates along the surface and in vertical $\sigma$ co-ordinate can be written in the following form:

$$\frac{\partial C}{\partial t}+\frac{\partial}{\partial \lambda}\left(\frac{u_\lambda}{R\cos\varphi}\cdot C\right)+\frac{\partial}{\partial \varphi}\left(\frac{u_\varphi}{R}C\right)+\frac{\partial}{\partial \sigma}\left(\dot{\sigma}\,C\right)=\frac{\partial}{\partial \sigma}\left\{\rho\,K_\sigma\,\frac{\partial}{\partial \sigma}\left(\frac{C}{\rho}\right)\right\}+Q \qquad (1.1)$$

where $C = C(\lambda,\varphi,\sigma)$ – concentration of pollutant (ng);

$\lambda$, $\varphi$ – geographic longitude and latitude (rad);

$u_\lambda(\lambda,\varphi,\sigma)$ – zonal component of wind speed (m/s);

$u_\varphi(\lambda,\varphi,\sigma)$ – meridional component of wind speed (m/s);

$\sigma = P/P_S$ – vertical $\sigma$ co-ordinate (Pa/Pa);

$P$ – atmospheric pressure at $\sigma$-level (Pa);

$P_S$ – surface pressure (Pa);

$\dot{\sigma}$ – analogue of the vertical velocity ($s^{-1}$):

$$\dot{\sigma} = \frac{\partial \sigma}{\partial t} + \frac{u_\lambda}{R\cos\varphi}\frac{\partial \sigma}{\partial \lambda} + \frac{u_\varphi}{R}\frac{\partial \sigma}{\partial \varphi} - \frac{\rho g}{P_S}w \qquad (1.2)$$

where $w$ – vertical velocity (m/s);

$K_\sigma$ – analogue of the vertical eddy diffusion coefficient ($s^{-1}$):

$$K_\sigma = \left(\rho\frac{g}{P_S}\right)^2 \cdot K_Z \qquad (1.3)$$

where $R$ – radius of the Earth (m);

$K_Z$ – vertical eddy diffusion coefficient ($m^2/s$);

$\rho$ – air density ($kg/m^3$);

$g$ – gravitational acceleration ($m/s^2$);

The last term Q in equation (1.1) denotes the following sources and sinks of a pollutant (ng/s) due to:

- emission;
- degradation in air;
- wet deposition of the gaseous phase;
- wet deposition of the particle bound phase.

The boundary conditions are defined as follows:

- the upper and lateral boundaries of the model domain are open for the exchange with the rest of the atmosphere;
- at the lower boundary pollutant fluxes are determined by processes of gaseous exchange between air and underlying surface and of dry deposition of the particle-bound phase of the pollutant.

To determine the latter fluxes equation (1.1) is to be completed with equations describing processes in other environmental compartments such as soil (sea and vegetation in future).

Equation (1.1) is solved using the splitting by the physical processes with the application of the following finite – difference numerical schemes:

- ASIMD advection scheme for horizontal advection [*Pekar*, 1996].
- Smolarkiewicz positive definite up-stream advection scheme for vertical advection [*Smolarkiewicz*, 1983].
- Implicit finite-difference scheme for vertical diffusion [*Samarsky*, 1977].

**Figure 1.2** Graphical representation of the modelling domain of hemispheric transport model

Modelling domain of the model covers the whole Northern Hemisphere. Within this domain the following three compartments are considered: air, soil and sea water. Sea/land mask is attached to every horizontal grid cell. The atmospheric part consists of 144x37 grid cells with gridsize 2.5º in horizontal direction. Vertical grid consists of 10 $\sigma$-levels $\sigma_k$ with grid steps $\Delta\sigma_k$, given in the Table 1.1.

**Table 1.1.** Vertical $\sigma$ co-ordinate system used in the model

| $\sigma_k$ | 0.99 | 0.96 | 0.91 | 0.85 | 0.77 | 0.68 | 0.59 | 0.40 | 0.26 | 0.1 |
|---|---|---|---|---|---|---|---|---|---|---|
| $\Delta\sigma_k$ | 0.02 | 0.04 | 0.06 | 0.06 | 0.1 | 0.08 | 0.1 | 0.16 | 0.16 | 0.16 |

The soil compartment consists of 5 vertical levels with depth of 0.5, 0.5, 1, 2 and 11 cm (layer depth increases in the downward direction), and the sea compartment consists of one vertical level of 25 m depth.

## 1.2. *Description of model atmospheric part*

### 1.2.1 Horizontal advection

The equation of horizontal advection in the spherical co-ordinate system has the following form (see equation 1.1):

$$\frac{\partial C(\lambda,\varphi,t)}{\partial t}+\frac{\partial}{\partial\lambda}\left(\frac{u_\lambda}{R\cos\varphi}C(\lambda,\varphi,t)\right)+\frac{\partial}{\partial\varphi}\left(\frac{u_\varphi}{R}C(\lambda,\varphi,t)\right)=0 \qquad (1.4)$$

where $u_\lambda = u_\lambda(\lambda,\varphi,\sigma)$, $u_\varphi = u_\varphi(\lambda,\varphi,\sigma)$ – zonal and meridional components of wind speed (m/s).

Equation (1.4) can be presented in the derived form:

$$\frac{\partial C}{\partial t}+\frac{\partial}{\partial\lambda}(uC)+\frac{\partial}{\partial\varphi}(vC)=0 \qquad (1.5)$$

where $u=\frac{u_\lambda}{R\cos\varphi}$ – derived zonal wind speed ($s^{-1}$);

$v=\frac{u_\varphi}{R}$ – derived meridional wind speed ($s^{-1}$).

Equation (1.5) has the form of the advection equation in the Cartesian co-ordinates and is solved using the ASIMD finite-difference advection scheme [*Pekar*, 1996].

The stability condition of the explicit advection scheme is:

$$|u_{i,j}|\Delta t \le h, \quad |v_{i,j}|\Delta t \le h, \quad h=\Delta\lambda=\Delta\varphi, \qquad 1\le i\le 144, \qquad 1\le j\le 37$$

where $h$ is the constant grid step, and $\Delta t$ – is the dynamic time step, which needs to be defined.

Using this stability condition one can determine a dynamic time step $\Delta t$ in the following way:

$$\Delta t = \tau / N \tag{1.6a}$$

$$N = \frac{\tau}{h / |U|_{\max}} \tag{1.6b}$$

where $\tau$ - is the time step of the main computation loop;

$|U|_{max}$ – maximum among all wind speed modules $|u_{i,j}|$ and $|v_{i,j}|$ ($1 \le i \le 144$, $1 \le j \le 37$).

### 1.2.2 Vertical advection

The equation of vertical advection in vertical $\sigma$ co-ordinate system has the following form:

$$\frac{\partial C(\sigma,t)}{\partial t} + \frac{\partial}{\partial \sigma}\left(\dot{\sigma} C(\sigma,t)\right) = 0 \tag{1.7}$$

where $\dot{\sigma}$ is defined by (1.2).

Vertical advection is calculated using Smolarkiewicz advection finite–difference scheme in the non-uniform grid [*Smolarkiewicz*, 1983].

### 1.2.3 Vertical diffusion

The equation of vertical diffusion in σ co-ordinate has the form (see equation 1.1):

$$\frac{\partial C(\sigma,t)}{\partial t} = \frac{\partial}{\partial \sigma}\left\{\rho K_\sigma \frac{\partial}{\partial \sigma}\left(\frac{C(\sigma,t)}{\rho}\right)\right\} \tag{1.8}$$

where $K_\sigma = \left(\frac{g}{P_S}\rho\right)^2 K_Z$.

Since the factor $\left(\frac{g}{P_S}\rho\right)$ has dimensions of $m^{-1}$, coefficient $K_\sigma$ has dimensions of $s^{-1}$.

Diffusion coefficient is determined at the cell boundaries. Equation (1.8) has a form of an ordinary diffusion equation. It is solved using an implicit finite-difference scheme, with the template presented in the Figure 1.3.

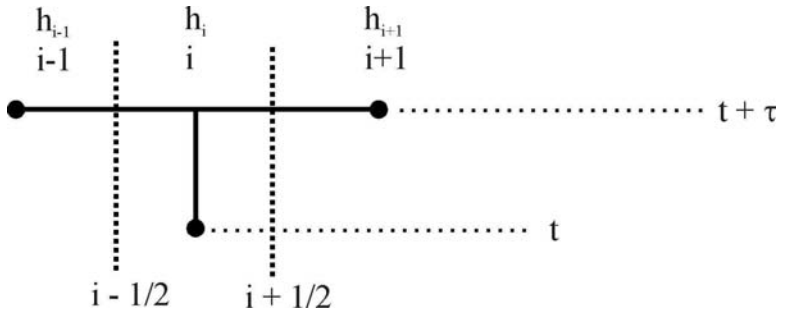


**Figure 1.3.** Implicit diffusion scheme template

The following notations are used on this Figure:

i, i-1, i+1 – numbers of the current, previous and next cells;
t – current time layer (s);
t+τ – new time layer (s);
τ – time step (s);
$h_i$, $h_{i-1}$, $h_{i+1}$ – sizes of the current, previous and next cells;
i-1/2 and i+1/2 – boundaries of the cell i.

On this template diffusion fluxes through the grid cell boundaries $F_{i-1/2}$ and $F_{i+1/2}$ are defined as:

$$F_{i-1/2} = \rho_{i-1/2} K_{i-1/2} \frac{(C/\rho)_i - (C/\rho)_{i-1}}{0.5(h_{i-1} + h_i)} \quad (1.9a)$$

$$F_{i+1/2} = \rho_{i+1/2} K_{i+1/2} \frac{(C/\rho)_{i+1} - (C/\rho)_i}{0.5(h_i + h_{i+1})} \quad (1.9b)$$

Here $h_i$ is the variable grid step, in this case it equals $\Delta\sigma_i$ , $1 \le i \le 10$.

Finite-difference approximation of equation (1.8) on the above template is:

$$\frac{C_i^{t+\tau} - C_i^t}{\tau} = \frac{F_{i+1/2}^{t+\tau} - F_{i-1/2}^{t+\tau}}{h_i} \quad (1.10)$$

where $C_i^t$ – concentration in the grid cell *i* at the time level *t*;
$C_i^{t+\tau}$ – concentration in the grid cell *i* at the time level $t + \tau$;
$F_{i+1/2}^{t+\tau}$ – flux across the right boundary of the grid cell *i*;
$F_{i-1/2}^{t+\tau}$ – flux across the left boundary of the grid cell *i*;
τ – time step,
$h_i$ – grid step (size of the cell) for the grid cell *i*.

Equations (1.9, 1.10) represent the implicit finite-difference scheme for diffusion equation. The system of equations (1.10) for ($1 \le i \le j$) with the properly defined boundary conditions is solved using sweep method.

### 1.2.4 Gas-particle partitioning in the atmosphere

Some of POPs occur in the atmosphere both in the gaseous phase and bound to particles. Therefore there is a need to include the process of partitioning between these two phases into the model. According to the Junge-Pankow model [*Junge*, 1977] POP fraction adsorbed on particle surfaces can be determined as follows:

$$\phi = \frac{c\theta}{p_L^0 + c\theta} \tag{1.11}$$

where $c$ – the constant dependent on thermodynamic parameters of the adsorption process and on the particle surface properties ($c$ = 0.17 Pa m [*Junge*, 1977]);

$p_L^0$ – subcooled liquid pressure (Pa);

$\theta$ – specific surface of aerosol particles.
($\theta$ = 1.5 $10^{-4}$ $m^2/m^3$ for background regions).

### 1.2.5 Wet deposition of the gaseous and particle bound phases

To define the scavenging of the gaseous phase with precipitation the equilibrium between the gaseous phase in the air and the dissolved phase in precipitation is assumed:

$$C_W^G = C_A^G / K_H \tag{1.12}$$

where $C_A^G$ - gaseous phase concentration in air ($ng/m^3$);

$C_W^G$ - dissolved phase concentration in precipitation ($ng/m^3$);

$K_H = K_H(T)$ - dimensionless Henry's law coefficient:

$$K_H = \frac{1}{RT} \cdot H = \frac{1}{RT} 10^{-\frac{A}{T}+B} \tag{1.13}$$

$H$ – Henry's law coefficient (Pa $m^3$ $mol^{-1}$), $A$ and $B$ – slope and the intercept peculiar of the individual POP;

$R$ – universal gas constant (8.31441 J $mol^{-1}$ $K^{-1}$).

Here $C_W^G$ means the concentration due to scavenging with precipitation not only in the current layer but also in the whole precipitation column lying above the current layer.

For the description of the particle bound phase scavenging with precipitation the washout ratio is used:

$$C_W^P = W_P C_A^P \tag{1.14}$$

where $C_A^P$ - particle bound phase concentration in air (ng/m$^3$);

$C_W^P$ - particle bound phase concentration in precipitation (ng/m$^3$);

$W_P$ - dimensionless washout ratio.

In this case $C_W^P$ means the concentration captured only with precipitation forming in the current layer.

### 1.2.6 Dry deposition of the particle bound phase

Dry deposition flux of the particle bound phase $F_{DRY}^P$ (ng m$^{-2}$ s$^{-1}$) is defined as:

$$F_{DRY}^P = C_A^P \cdot V_d \tag{1.15}$$

where $C_A^P$ - concentration of the particle bound phase in the air surface layer (ng/m$^3$);

$V_d$ - dry deposition velocity of particles (m/s).

The value of dry deposition velocity depends on particle type and on some surface layer parameters namely: friction velocity $u_*$ (m/s) and surface roughness $z_0$(mm). *M.Pekar* (1996) has obtained the following expressions for dry deposition velocities over the land and sea on the basis of the semi-empirical model of [*Sehmel*, 1980].

$$V_d^{LAND} = \left(A^{LAND} \cdot u_*^2 + B^{LAND}\right) \cdot z_0^n \qquad \text{(cm/s)} \tag{1.16a}$$

$$V_d^{SEA} = A^{SEA} \cdot u_*^2 + B^{SEA} \qquad \text{(cm/s)} \tag{1.16b}$$

The values of coefficients used in formulas (1.16 a,b) for different particle sizes are presented in Table 1.2.

**Table 1.2.** Coefficients for computation of dry deposition velocity over land and sea for two particle diameters

| Particle diameter, μm | $A^{LAND}$ | $B^{LAND}$ | n | $A^{SEA}$ | $B^{SEA}$ |
|---|---|---|---|---|---|
| d = 0.84 | 0.04 | 0.02 | 0.3 | 0.15 | 0.023 |
| d = 0.55 | 0.02 | 0.01 | 0.33 | 0.15 | 0.013 |

### 1.2.7 Parameterisation of the atmospheric boundary layer

The parameters of atmospheric boundary layer (vertical eddy diffusion coefficient, Monin-Obukhov length, and friction velocity) are prepared for the hemispheric modelling by SDA system (see chapter 2 of the report). However, the model provides the possibility to use meteorological data sets from other sources with limited number of parameters. For this the following calculation scheme of atmospheric boundary layer parameters can be used.

The vertical eddy diffusion coefficient $K_z$ ($m^2/s$) in the atmospheric boundary layer is specified as follows (adapted from [*Pekar et al.*, 1998]):

for unstable stratification:

$$K_z(z) = \frac{\kappa u_* z}{0.74} \cdot \sqrt{1 - 9\frac{z}{L}} \cdot \exp\left\{-\frac{4z}{H_{BL}}\right\} \qquad (1.17a)$$

for stable and neutral stratification:

$$K_Z(z) = \frac{\kappa u_* z}{0.74 + 4.7\frac{z}{L}} \cdot \exp\left\{-\frac{z}{H_{BL}}\right\} \qquad (1.17b)$$

where $\kappa$ – Von Karman constant (≈0.4);

$u_*$ – friction velocity (m/s),

L – Monin-Obukhov length (m),

$H_{BL}$ – the atmospheric boundary-layer height (m).

Above the boundary layer vertical eddy diffusion coefficient is specified equal to 0.2 $m^2/s$.

Friction velocity $u_*$ is set according to the formula [*Bizova et al. ,*1987]:

$$u_* = \frac{\kappa u_{10}}{\ln\left(\frac{10}{z_0}\right) + A_P} \tag{1.18}$$

where $u_{10}$ – wind speed at 10 (m/s);

$z_0$ – roughness parameter (m);

$A_P$ – parameter depending on Pasquill-Gifford-Turner (PGT) stability class A-F (Table 1.3):

**Table 1.3.** Pasquill-Gifford-Turner (PGT) stability classes A-F

| PGT stability class | A | B | C | D | E | F |
|---|---|---|---|---|---|---|
| $A_P$ | -0.7 | -0.5 | -0.3 | 0.1 | 0.3 | 0.8 |

The similarity functions for heat are defined as follows:

For unstable stratification:

$$\Psi_h\left(\frac{z}{L}\right) = 2 \cdot ln\frac{1+x}{2}, \quad x = \sqrt{1-15\frac{z}{L}}\,. \tag{1.19a}$$

For stable and neutral stratification:

$$\Psi_h\left(\frac{z}{L}\right) = -4.7\frac{z}{L}. \tag{1.19b}$$

## 1.3. *Degradation processes*

Degradation processes in all media considered in the model are described as the first order processes different for different compartments and pollutants. Degradation of a pollutant in each media can be defined by the following equation:

$$C^{t+\Delta t} = C^t \cdot \exp\left\{-k \cdot \Delta t\right\} \tag{1.20}$$

where $C^t, C^{t+\Delta t}$ - pollutant concentration in the media at the times t and t+$\Delta$t;

$k$ = 1/$\tau$ – degradation rate in particular compartment ($s^{-1}$),

$\tau$ – life time in particular compartment;

$\Delta$t – degradation time (s).

## 1.4. *Gaseous exchange with underlying surface*

The gaseous exchange with the underlying surface (soil and sea) along with POP transport processes in soil is described according to the model of *C.M.J.Jacobs and W.A.J.van Pul* [1996]. The appropriate program units has been developed in RIVM and made available to MSC-E together with parameterization and initial data. The parameterization of the gaseous exchange process between the air and underlying surface (soil and sea) is realized with the resistance analogy (Figure 1.4).

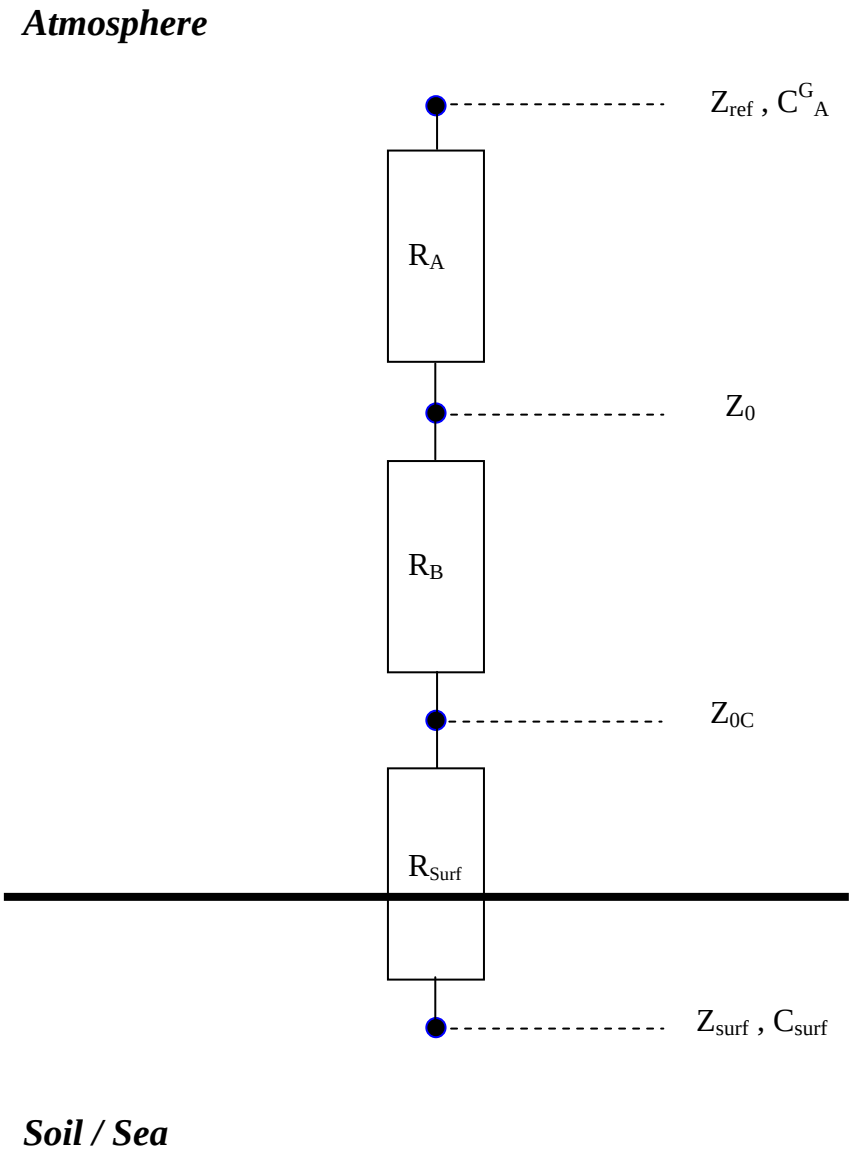


**Figure 1.4.** Schematic representation of the surface-atmosphere exchange

On this Figure the following notations are used:

$z_{ref}$ – reference height (50 m),

$z_0$ – roughness height,

$z_{0C}$ – average source or sink height,

$R_A$ – aerodynamic resistance between the reference height and roughness height,

$R_B$ – boundary-layer resistance between the roughness height and average source or sink height,

$R_{surf}$ – surface resistance,

$C^G_A$ – gas phase concentration at the reference height,

$C_{surf}$ – surface concentration in the top layer of the soil or sea.

The gaseous flux from the atmosphere to soil (sea) $F^G_{DRY}$ is defined in the following way:

$$F^G_{DRY} = \frac{C^G_A - C_{surf}}{R_A + R_B + R_{surf}} \tag{1.21}$$

The resistance of the atmospheric surface layer to gas exchange $R_{AB} = R_A + R_B$ is defined as:

$$R_{AB} = \frac{\ln\left(\frac{z_{ref}}{z_0}\right) - \Psi_h\left(\frac{z_{ref}}{L}\right) + \Psi_h\left(\frac{z_0}{L}\right)}{\kappa u_*} + \frac{2}{\kappa u_*}\left(\frac{Sc}{\mathrm{Pr}}\right)^{2/3} \tag{1.22}$$

where $S_c$ – Schmidt number, which is the ratio of air kinematic viscosity ($0.2\times10^{-5}$ m$^2$/s) to the coefficient of pollutant molecular diffusion in air;

$P_r$ – Prandtl number (0.72);

$\Psi_h$ ($z/L$) – similarity function for heat ( eq. 1.19).

# 2. *Description of the system supplying meteorological information for modelling*

To provide the pollution long-range transport modelling with meteorological information a special system was developed by Hydrometeorological Centre of Russia. This System of Diagnosis of the lower Atmosphere (SDA) is based on the experience gained in the development and maintaining of the system of meteorological information supply for regional HM and POP transport models of EMEP/MSC-E [*Frolov et al.*, 1994; *Rubinstein et al*., 1997,1998; *Frolov et al.*, 1997 (1,2,3)].

The SDA system provides a broader list of meteorological parameters (Table 2.1) in comparison with previous approach and it uses series of accumulated objective analyses. Below we will briefly describe main features of SDA, its main units and meteorological information obtained for 1990.

## 2.1. *Description of SDA basic principles*

The main task of the developed SDA system is to provide a set of meteorological parameters and the spatial structure defined according to the requirements of hemispheric and regional multi-compartment models being developed at EMEP/MSC-E. The list of these parameters is presented in Table 2.1.

This system provides meteorological information for the Northern Hemisphere on the basis of the objective analysis of meteorological fields and data on the oceanic surface temperature fields. Since the major part of the parameters in Table 2.1 are not measurable and hence are not included in the results of the objective analysis, one of the main unit of SDA system is the hydrodynamic prognostic model. This model is used not only to provide missing parameters but also to provide temporal resolution required for atmospheric transport models. For regional pollution transport models where finer spatial resolution is needed a set of specially developed procedures of “downscaling” has been developed.

**Table 2.1** List of meteorological parameters on longitude-latitude grid for the Northern Hemisphere with resolution of 2.5ºx2.5º

| Element | Units | Type | Levels |
|---|---|---|---|
| 1. Wind velocity (zonal component) | m/s | Instantaneous | 10 levels (Table 1.1) |
| 2. Wind velocity (meridional component) | m/s | Instantaneous | 10 levels (Table 1.1) |
| 3. Analogue of vertical velocity in sigma-coordinate system (at the upper boundary of the layer) | 1/s | Instantaneous | 10 levels (at layer boundaries) |
| 4. Geopotential height | dkm | Instantaneous | 10 levels (Table 1.1) |
| 5. Temperature | K | Instantaneous | 10 levels (Table 1.1) |
| 6. Water vapor mixing ratio | g/g | Instantaneous | 10 levels (Table 1.1) |
| 7. Large-scale cloudiness | ball | Mean 6 hours | 10 levels (Table 1.1) |
| 8. Convective cloudiness | ball | Mean 6 hours | 10 levels (Table 1.1) |
| 9. Precipitation | m/6 hours | Accumulated during 6 hours | 10 levels (Table 1.1) |
| 10. Coefficient of vertical turbulence | $m^2/s$ | Instantaneous | 4 lower levels (Table 1.1) |
| 11. Monin-Obukhov length | m | Instantaneous | surface |
| 12. Friction velocity | | Instantaneous | surface |
| 13. Surface pressure | hPa | Instantaneous | surface |
| 14. Surface temperature | K | Instantaneous | surface |
| 15. Level of roughness | m | Instantaneous | surface |
| 16. Soil moisture on surface | m | Instantaneous | surface |
| 17. Snow cover height | m | Instantaneous | surface |

At present in accordance with modelling requirements meteorological data for 1990 are obtained using the developed SDA system.

The main units of SDA technological system are the following:

- unit of initial data preparation including the control and correction of errors,
- unit of preparation of boundary conditions,
- computational unit with the use of the hydrodynamic prognostic model,
- post-processing unit including the computations of the boundary layer parameters.

## 2.2. *SDA technological scheme*

In the realized system the preparation of data is made according to the following main steps:

- Preparation of the meteorological information for the Northern Hemisphere;
- Preparation of the meteorological information for the EMEP domain;
- Corrections of the results on the basis of observational data.

Below more detailed description of problems solved at each step is given.

### *Preparation of the meteorological information for the Northern Hemisphere*

- The preparation of an annual set of initial information. As initial information gridded data obtained by objective analysis made by Hydrometeorological Centre of Russia or by reanalysis of NCAR/NCEP are used. These data include horizontal wind components, temperature, and humidity on the standard isobaric surfaces with 12-hour interval. Initial data can have some gaps and errors. For this case the special procedure was developed for the control and correction of possible errors in initial data.
- As the next step the hydrodynamic prognostic model of Hydrometeorological Centre of Russia (version T40L15) is run for 12-hour period with the initial data based on the previous step results and data of weekly analysis of the sea surface temperature and sea ice distribution. Modelling results are recorded for each 6-hour interval.
- To obtain the initial data for the next model run the prognostic fields produced by the model are mixed with results of the objective analysis. Weighted multipliers for each type of the field are specially selected by a number of numerical experiments.
- Computed meteorological parameters are interpolated to the required spatial structure (horizontal and vertical).
- In the new spatial structure diagnostic calculations of the analogue of vertical velocity and all the parameters of the boundary layer are performed.
- The data are aggregated according to periods (4 periods round the clock) with possible subsequent compression.
- As the final step the analysis and control of the output meteorological information is performed.

In the framework of SDA system a special procedure of downscaling of meteorological data to a sub-region is envisaged. The data for the Northern Hemisphere are used as the initial data. In the free atmosphere (above the planetary boundary layer) scalar values are interpolated from

the large-scale grid to small-scale grid. Within the boundary layer all scalar parameters are calculated with allowance for more detailed orography and surface properties.

For the adjustment of the wind fields the procedure of variation three-dimensional agreement is used with more detailed orography. This procedure is based on minimization of standard deviation of the modified fields from the initial one under the condition of conservation of divergence of the initial field and flowing round an obstacle.

*Correction of results using observational data*

In calculations of a number of meteorological parameters in SDA system observational data are not used, i.e. these parameters are purely model ones. Thus the parameters are, for example, precipitation, land surface temperature, snow cover thickness, soil moisture, cloudiness etc. On the other hand, for some parameters there are series of observations. For example, for each observation period there are thousands of precipitation measurements in the Northern Hemisphere. At present the procedure is being developed which will allow to correct precipitation over the land of the Northern Hemisphere using observational data.

Below three main SDA units will be briefly described, namely: the hydrodynamic prognostic model of Hydrometerological Centre of Russia, the use of special archive of data on sea surface temperature and sea ice distribution and computation of the boundary layer parameters.

## 2.3. *Description of hydrodynamic prognostic model*

This model described in [*Kurbatkin et al.*, 1994] is based on numerical integration of a set of hydrodynamic equations for baroclinic atmosphere in quasi-static approximation. Along the vertical $\sigma$ co-ordinate is used, where $\sigma = P/P_S$ , P – atmospheric pressure and $P_S$ – surface pressure. The equation set is solved by the spectral method with triangle truncation on the hemispheric scale in the atmospheric layer between the Earth surface ($\sigma = 1$) and the upper level ($\sigma = 0$). At the upper and lower boundaries kinematic conditions are prescribed:

$\dot{\sigma} = 0$ at $\sigma = 0$ and $\sigma = 1$

and at $\sigma = 0$ also the condition of absence of heat, moisture and impulse fluxes is used.

The computations are carried out by T40 version of the model corresponding to the spatial resolution 2.5 degree on Gaussian (non-uniform along latitude) grid. Along the vertical the

atmosphere is divided into 15 layers. Basic prognostic and diagnostic variables of the model are calculated for the middle of each layer. Values of vertical velocity analogues and radiation fluxes are calculated at the layer boundaries. Specific σ values at the basic model levels are presented in Table 2.2.

**Table 2.2.** Level numbers and σ values in the middle of the layers

| ***N*** | ***15*** | ***14*** | ***13*** | ***12*** | ***11*** | ***10*** | ***9*** | ***8*** |
|---|---|---|---|---|---|---|---|---|
| σ | 0.99 | 0.96 | 0.91 | 0.85 | 0.77 | 0.68 | 0.59 | 0.5 |
| ***N*** | ***7*** | ***6*** | ***5*** | ***4*** | ***3*** | ***2*** | ***1*** | |
| σ | 0.45 | 0.34 | 0.26 | 0.19 | 0.15 | 0.07 | 0.05 | |

As the scheme of integration over time the semi-implicit scheme of Nemchinova-Sadokova-Rober is used.

This model considers basic physical processes within the atmosphere and at the underlying land surface important for large-scale numerical weather forecast and atmospheric circulation modelling. Below a brief description of these processes will be given.

### *Horizontal macroturbulence*

For the parametrization of horizontal turbulence processes a linear scheme of a fourth order is used. In this model version it is assumed that the horizontal diffusion coefficient has the following value: $K_H = 8 \times 10^{14}$ $m^2 s^{-1}$.

### *Vertical diffusion transport*

In the free atmosphere fluxes of the impulse, enthalpy and moisture are calculated on the basis of *K*-theory. The coefficient of vertical turbulence is determined by the hypothesis on mixing route. It is supposed that this coefficient depends on the wind shear and static stability.

### *Large-scale condensation*

The parametrization is based on the fact that precipitation takes place when the humidity exceeds critical values which for “warm” clouds (with the temperature at the upper boundary higher than $-12^0$C) is 2 g/kg. In subcooled clouds all the condensed moisture precipitates. Besides the effect of rain drops evaporation is taken into account and corrections for negative humidity values resulted from approximation errors are made.

*Convective processes*

In the parametrization of wet convective processes the scheme of Kyo penetrating convection is used. Vertical and horizontal convective turbulent fluxes of the impulse, enthalpy and moisture are not considered in this version of the model, since it is supposed, that their impact on the atmospheric circulation is negligible.

*Solar radiation*

The parametrization scheme for radiation processes considers main effects of solar radiation on the atmosphere and ground surface. The effect of cloudiness and aerosol are considered in detail. The lower troposphere is the field of main interests in view of supplying with data for modelling of pollutant transport. For the lower troposphere the diurnal variation plays an essential role in the reproduction of circulation. It inflicts a considerable impact on near surface processes and therefore it is introduced in daily and annual variations of short-wave radiation.

*Calculations of land surface temperature*

In the model temperature of the land surface is a prognostic variable. It is assumed that land is represented by a thin layer (42 cm) of soil where the local exchange by moisture and heat with the atmosphere takes place. Temperature is calculated on the basis of heat balance conditions.

*Parametrization of land hydrology*

It is assumed that soil is divided into two layers. While calculating moisture variations in the upper soil layer, snow melting, moisture input due to precipitation and its diminishing due to evaporation as well as diffusive exchange with the lower layer are taken into account. The horizontal transport of moisture in soil is absent.

As lower boundary conditions we use fields of the surface temperature (recalculated in the computation process), ocean surface temperature (prescribed, see below), temperature at the depth of $D$=0.42 m ($T_D$) (prescribed), soil moisture content (recalculated in the computation process), snow cover height (prescribed, see below). In addition, fields of the roughness height and surface albedo (corrected for ice and snow in the course of computations) are used.

## 2.4. *Special archive of data on sea surface temperature and sea ice distribution*

In modelling the general atmospheric circulation and numerical weather forecast it is necessary to prescribe appropriate boundary conditions, in particular, data on sea surface temperature and sea ice distribution. The main problem is connected first of all with lack of synchrony between variations in the atmosphere and on the underlying surface. It is expedient to use diagnostic fields of the ocean surface temperature and sea ice distribution in the system of computation of meteorological fields for modelling of pollutant transport on the hemispheric and regional scales.

For this purpose a special archive of data and the appropriate program-technological interface with the computation system using the prognostic model have been developed. Among operational diagnosis of the least temporal discreteness, the products of the National Centre on Environment Prediction (the USA NCEP/NOAA) is distinguished. The Centre provides weekly analysis of the ocean surface temperature for the whole World Ocean in the geographical grid with spatial resolution $1^{o}x1^{o}$ with the consideration of the boundary position of the ice cover [*Reynolds and Smith*, 1994]. Since in computation with the atmospheric model the data can be renewed every day and even from one period to another, then the archive should meet the requirement of regularity (smoothness) of fields interpolated relative to time. Another requirement is connected with a rapid excess to fields with arbitrary prescribed time period.

## 2.5. *Computation of boundary layer parameters*

The main task of computation of boundary layer parameters is the definition of vertical structure of meteorological variables inside the atmospheric boundary layer (ABL), up to the height about 1500 m and computation vertical turbulent diffusion coefficients on four lower levels, dynamic near surface velocity, and Monin-Obukhov parameter.

The planetary atmospheric boundary layer (ABL) is separated as a peculiar part of the atmosphere differed from the free atmosphere by the following peculiarities:

- essentially higher than in other parts of the atmosphere vertical gradients of meteorological parameters (wind speed, temperature, air humidity);
- developed regime of the small-scale turbulent mixing;
- distinctive diurnal variation of meteorological parameters.

Due to viscous adhering of the air flux on the ground surface there arise vertical velocity gradients exceeding critical values for the transition from the laminar regime to the turbulent one.

From the dynamic point of view ABL differs from the free atmosphere by the balance of main forces in the equation of motion.

Turbulent mixing being one of main factors of the ABL structure formation affects the redistribution of any other substance: gaseous pollutants, aerosols, etc.

In the lower ABL with the thickness of several tens of meters a near surface (water) sublayer is distinguished where an essential part of vertical variations of substances of the whole ABL take place. Vertical turbulent fluxes are almost independent of height and wind, temperature and humidity profile they are close to logarithmic one. The structure of the surface layer is described using Monin-Obukhov similarity theory.

The problem is to determine the vertical structure of ABL at the prescribed at its boundaries meteorological variables (horizontal wind speed components (u,v), air temperature T and its specific humidity q):

ABL upper boundary:

$z = h \sim 1500$ m ($\sim$850 hPa): $u = u_h, \quad v = v_h$ (2.1)
$T = T_h$
$q = q_h$

underlying surface,

$z = 0$ (or $z = z_0$ – roughness level) $u = 0, \quad v = 0$ (2.2)
$T = T_0$
$q = q_0$

We proceed from the assumption that fields of wind speed, temperature and air humidity are statistically stationary and statistically uniform along the horizontal. It was also assumed that within ABL it is possible to neglect vertical variations of radiation heat flux. On these assumptions all one-point statistical characteristic of meteorological fields (mean values of $u$, $v$, $T$, $q$ and characteristic of turbulence) should be directly dependent only on the height above the underlying surface. Functional expressions for these dependencies are determined from equations for momentum, heat and moisture transport. Hence the formulated model can be interpreted as a hydrodynamic interpolator of meteorological variables within ABL.

Traditionally equations for ABL refer to z-coordinate system where vertical distances are determined in geometrical units. At the same time the system supplying pollution transport models with meteorological information uses $\sigma$-levels. In this connection ABL equations are rewritten in the $\sigma$-system.

The problem is solved with the iteration method with subsequent determination of coefficients dependent on the solution of the system. The iteration process is continued until the difference between solutions on the two subsequent iterations is less than a small threshold level.

The choice of a number of layers inside ABL for numerical solving of the initial system is done in the course of numerical experiments. Due to large vertical gradients of the ABL parameters it is necessary to use 10 layers for appropriate approximation.

## 2.6. *Illustration of meteorological information for 1990*

For the illustration of the operation of meteorological information supply system SDA we present data on precipitation and mean monthly wind fields. Figure 2.1 demonstrates the spatial distribution of precipitation amount for 1990 obtained by SDA.

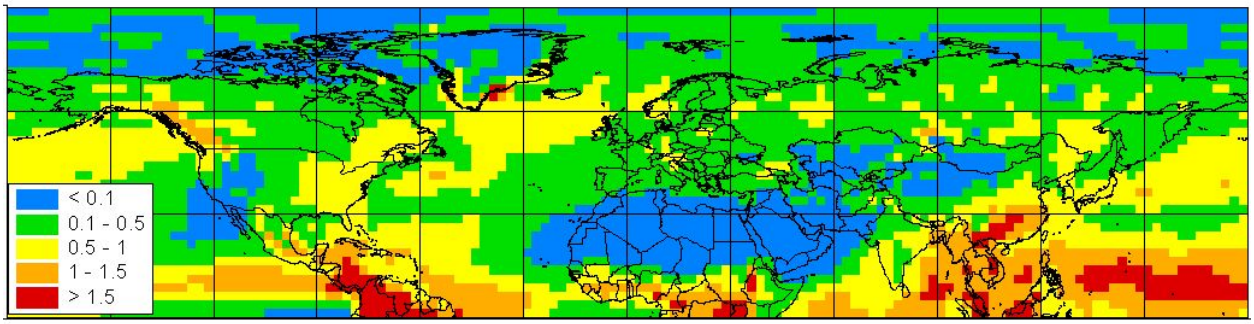


**Figure 2.1.** Spatial distribution of precipitation amount within the Northern Hemisphere in 1990 (m)

Figure 2.2 demonstrates the comparison of precipitation intensity obtained by SDA with observations obtained on the basis of ground measurements and satellite data for oceans (GPCP data [*Rudolf*, 1993]). These data were averaged over longitudes for January, April, July, and November of 1990. It is evident that general configuration and values of precipitation quite agree with observations. At same time SDA provided less intensive precipitation for spring-summer months in internal tropical convergence zone (ITCZ) - near the equator.

Figure 2.3 illustrates mean monthly wind velocity fields at the level $\sigma = 0.85$ (close to 850 mB) produced by SDA and obtained from NCAR/NCEP re-analysis data. It can be seen that the wind fields at the upper limit of the boundary layer obtained by SDA and from re-analysis data are in a reasonable agreement.

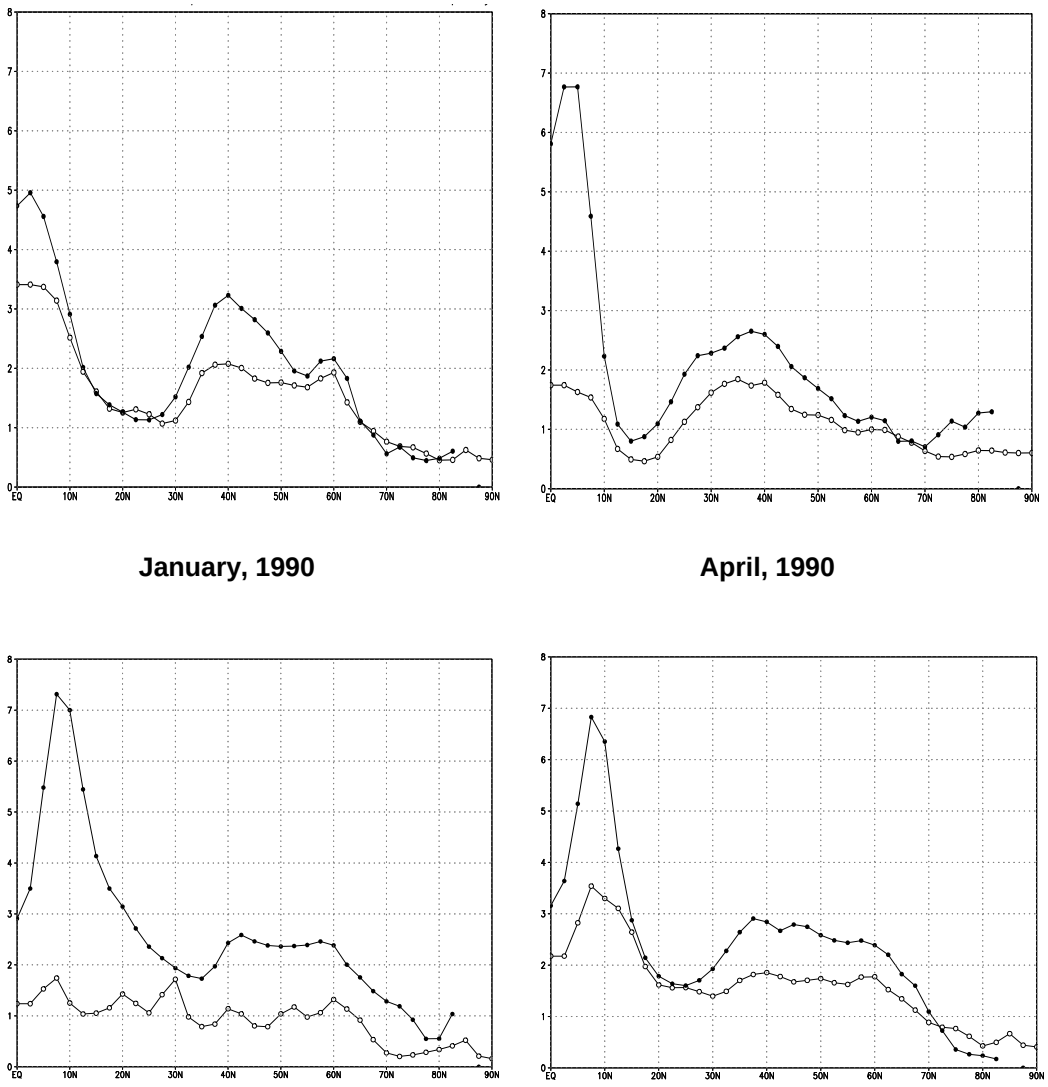


**Figure 2.2** Mean monthly precipitation intensity averaged over longitudes (mm/day). Comparison of SDA precipitation with observations from GPCP archive for 1990

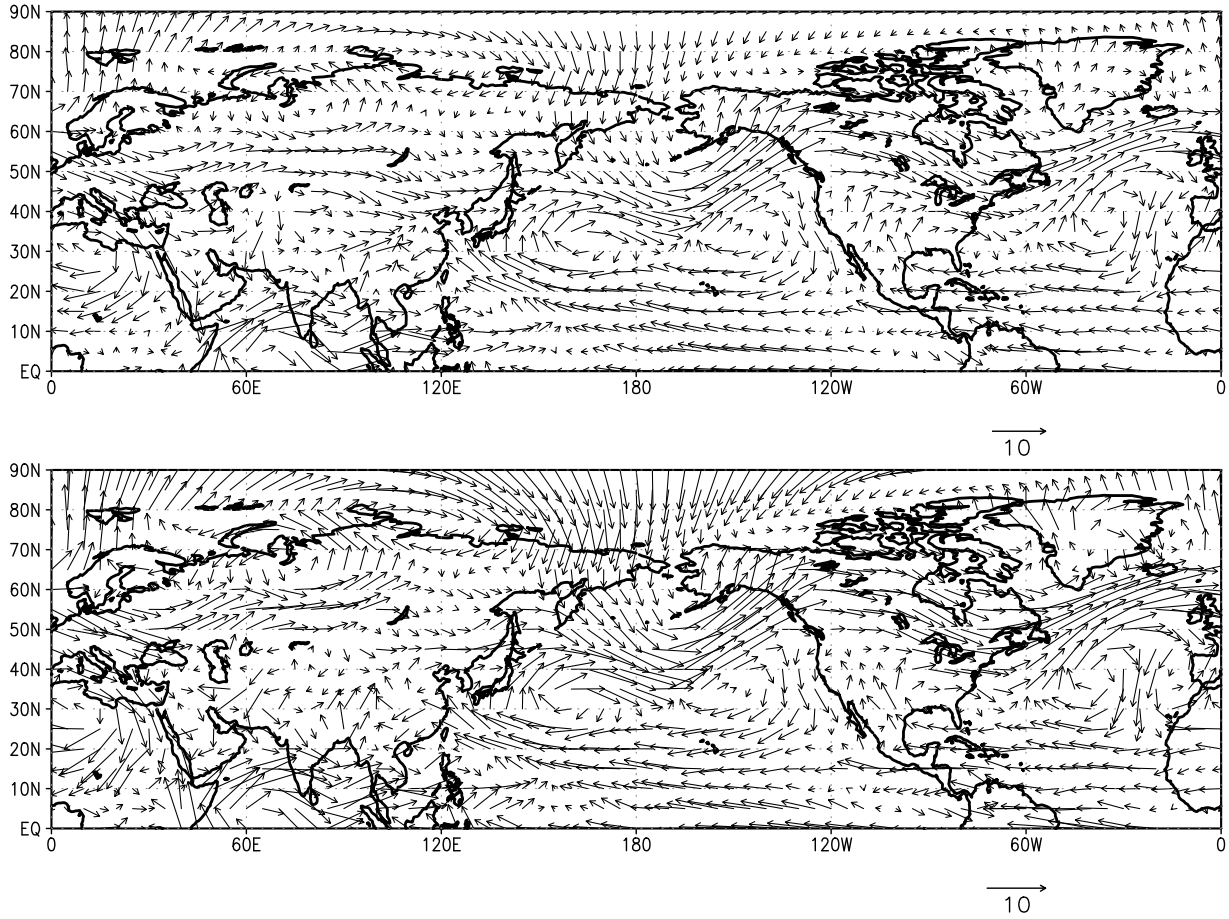


**Figure 2.3** Mean monthly wind fields at $\sigma$ = 0.85 for September 1990 obtained by SDA (upper diagram) and NCAR/NCEP re-analysis (lower diagram) (m/s)

# 3. *Results of modelling experiments*

Several modelling experiments were made to test the performance of the developed model. These experiments were focused mainly on the processes of the atmospheric transport of pollutants. The model was applied to simulation of the long-range transport of α-hexachlorocyclohexane (α-HCH) and polychlorinated biphenyls (PCBs) within the Northern Hemisphere. Modelling results for α-HCH were compared with available measurement data. Results for PCBs were compared with those of the regional model developed at MSC-E and described in [*Pekar et al.*, 1998; *Pekar et al.*, 1999]. This chapter presents a description of the input data and preliminary modelling results.

## 3.1. *Simulation of α-HCH long-range transport*

A simulation of α-HCH long-range transport within the Northern Hemisphere was chosen because of global emission data were available for this pesticide. This provides a possibility to analyse how the model reproduces distribution of a pollutant on the hemispheric scale. The model was run for meteorological situation of 1990 and with emission data for the same year. Meteorological data were obtained using the system of meteorological data supply described in chapter 2. Initial concentrations of α-HCH in all model compartments were assumed to be zero. Additional run was made for a 10-year period with one and the same meteorological data for 1990 and using global emission data for 1980 (during the first five years) and for 1990 (during the last five years), see Figure 3.9 below.

### 3.1.1 Physical-chemical properties of α-HCH

HCH (Hexachlorocyclohexane) is one of organochlorine pesticides. It has been extensively used in the world as an insecticide. Two of its isomers α– and γ–HCH had the most extensive usage. They have relatively high volatility and persistence. Therefore they can quickly evaporate into the atmosphere after the application and be transported far from their sources. For the modelling purpose a set of physical-chemical properties of α-HCH was prepared on the basis of the data obtained from literature (Table 3.1). It should be noted that the physical-chemical properties of α-HCH were not the subject of this study and were used to test the overall model functioning.

**Table 3.1.** Physical-chemical properties of α-HCH used for computations

| Characteristic | Value | Dimensions | Reference |
|---|---|---|---|
| Henry's law constant | $\log H = -\frac{3298}{T} + 10.88$ | Pa $m^3$ $mol^{-1}$ | [*Pacyna*, 1999] |
| Subcooled liquid pressure | $\log p_L^0 = -\frac{3575}{T} + 11.34$ | Pa | [*Pacyna*, 1999] |
| Washout ratio for particle bound phase | $W_P = 4\ 10^4$ | - | [*Pekar et al.*, 1999] |
| Octanol-water partition coefficient | Log $K_{OW}$ = 3.81 | - | [*Pacyna*, 1999] |
| Organic C partition coefficient | Log $K_{OC}$ = 2.65 | $m^3\ kg^{-1}$ | [*Pacyna*, 1999] |
| Degradation rate in air at 25°C | $K_{Aref} = 1.47\ 10^{-7}$ | $s^{-1}$ | [*Pacyna*, 1999] |
| Degradation rate in soil at 25°C | $K_{Sref} = 8.79\ 10^{-8}$ | $s^{-1}$ | [*Pacyna*, 1999] |
| Degradation rate in sea at 25°C | $K_{Wref} = 2.2\ 10^{-8}$ | $s^{-1}$ | [*Pacyna*, 1999] |
| Molecular diffusivity in air | $5.0\ 10^{-6}$ | $m^{-2}\ s^{-1}$ | [*Strand and Hov*, 1996] |
| Molecular diffusivity in water | $5.0\ 10^{-10}$ | $m^{-2}\ s^{-1}$ | [*Strand and Hov*, 1996] |

Note that in accordance with the accepted parameterization and Junge-Pankow model (see section 1.2.4) the fraction of the particulate phase for different temperatures is negligible (Table 3.2).

**Table 3.2.** Fraction of the particulate phase for α-HCH at different temperatures.

| Temperature (C) | 0 | 10 | 20 | 30 |
|---|---|---|---|---|
| Particulate fraction of α-HCH (%) | 0.14 | 0.05 | 0.02 | 0.007 |

According to the data presented in this Table it is possible to take into account only α-HCH gaseous phase for modelling.

### 3.1.2 Emission of α-HCH

Modelling of α-HCH hemispheric transport was carried out using the global emission data for 1980 and 1990 [*Li Y.F.*, 1999]. According to these estimates total consumption of α-HCH amounts to 184 kilotonnes in 1980 and 44.1 kilotonnes in 1990. The major α-HCH emission sources are located within the Northern Hemisphere. It was assumed that α-HCH emissions have the following seasonal variations: 10% in February, 15% in March, 25% in April, 25% in May and 25% in June.

**Table 3.3.** Estimates of α-HCH emissions for 1980 and 1990 (in tonnes)

| | Global emission | Northern hemisphere emission |
|---|---|---|
| 1980 | $1.840\ 10^5$ | $1.726\ 10^5$ |
| 1990 | $4.409\ 10^4$ | $4.013\ 10^4$ |

The spatial distribution of α-HCH emissions in 1980 and 1990 over the Northern Hemisphere is shown on Figure 3.1. Table 3.3 presents estimates of total α-HCH emissions within the Northern Hemisphere and on the global scale. It can be noted that as follows from these estimates α-HCH emissions were significantly reduced from 1980 to 1990.

**Figure 3.1.** Spatial distribution of α-HCH emissions over the Northern Hemisphere for 1980 (upper map) and 1990 (lower map) (tonnes/cell/yr)

### 3.1.3 Modelling results for 1990

Mean annual air concentrations of α-HCH in atmospheric surface layer for 1990 are shown

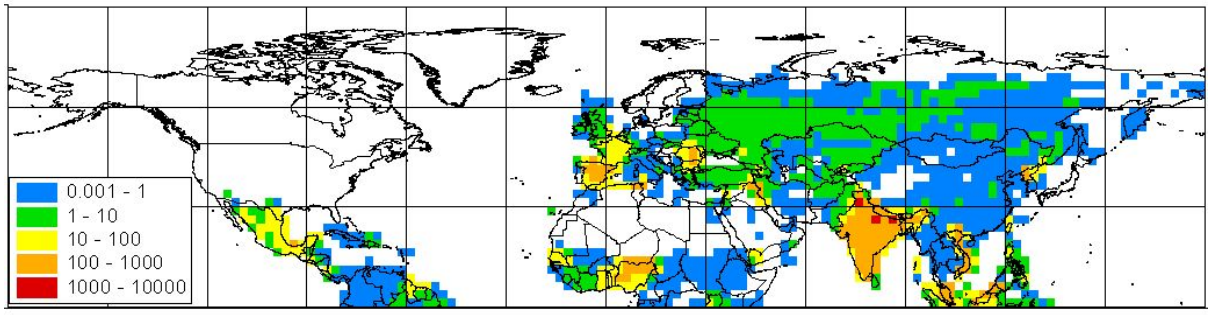


on Figure 3.2. The distribution of α-HCH concentrations reflects the main directions of the atmospheric long-range transport in the Northern Hemisphere. Thus in northern midlatitudes over Europe and Asia the prevailing transport direction is from the west to the east. From south-eastern Asian sources the pollutant is transported with air masses in the north-east direction to North America and with westerly winds across the Pacific Ocean. The highest air concentrations of α-HCH are obtained near the major emission sources located in South-east Asia, Africa and Europe. On the whole, the comparison of mean annual air concentrations of α-HCH with available observations demonstrates a reasonable agreement between them. However, in some regions of the Northern Hemisphere computed concentrations are several times higher than measured ones (Table 3.4). These discrepancies can be connected with a simplified description of exchange processes with the underlying surface and uncertainties of emission data.

**Table 3.4.** Comparison of computed and measured air concentrations of α-HCH (pg $m^{-3}$)

| Region | Observed | Computed | Reference |
|---|---|---|---|
| Northern North Pacific | 22 – 1300 | 0 – 2500 | [*Iwata et al.*, 1993] |
| North Atlantic | 87 – 320 | 0 – 1000 | [*Iwata et al.*, 1993] |
| Bay of Bengal and Arabian Sea | 570 – 29000 | 1000 – 50000 | [*Iwata et al.*, 1993] |
| Bering and Chukchi Seas | 144 – 408 | 0 – 1000 | [*Hinckley et al.*, 1991] |

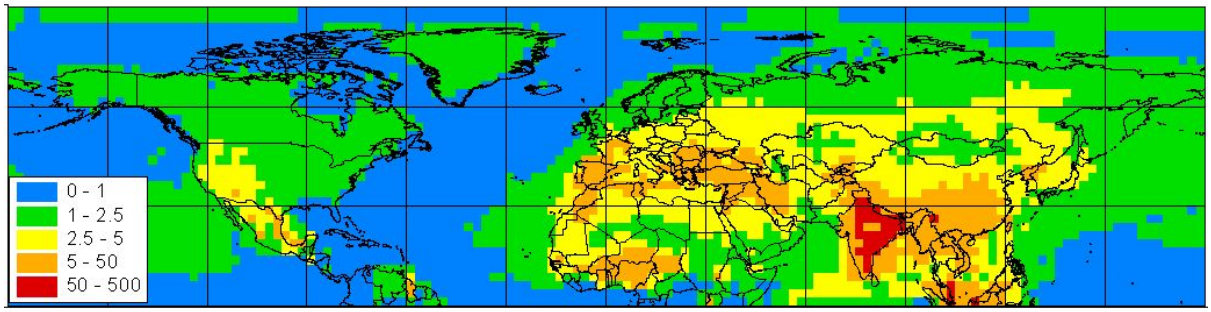


**Figure 3.2.** Spatial distribution of α-HCH mean annual air concentrations over the Northern Hemisphere in 1990 (ng $m^{-3}$)

Figure 3.3 presents the spatial distribution of total annual α-HCH depositions in 1990. It can be seen that deposition density in general is more intensive at the high latitudes (except for regions with high emissions). This can be connected with the known cold condensation effect described in [*Wania and Mackay*, 1995].

Further, there are some regions (in Bering Sea and Sea of Okhotsk) where annual re-emission flux exceeds depositions. However, as we shall see later re-emission flux from sea surface in other regions also takes place but mainly during the second half of the year (Figures 3.8 – 3.11).

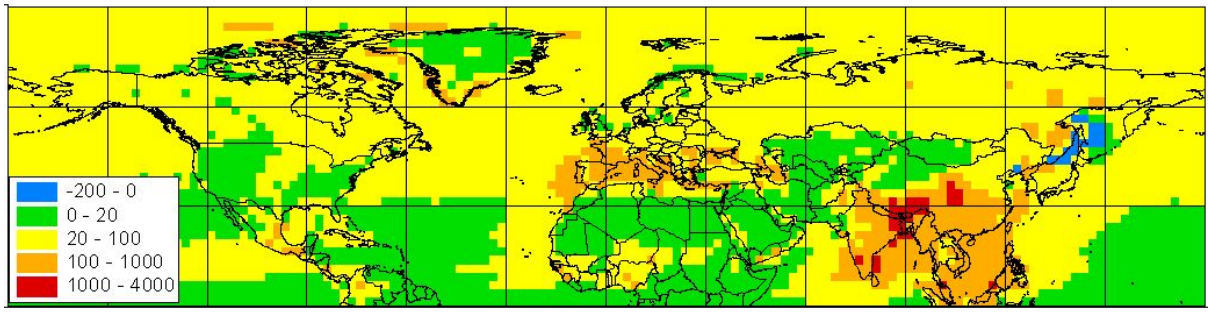


**Figure 3.3.** Spatial distribution of α-HCH total depositions within the Northern Hemisphere in 1990 (ng $m^{-2}$ $yr^{-1}$)

Figure 3.4 demonstrates the mass balance of α-HCH after simulation for 1990. The most significant part of emitted α-HCH degraded in air (40%), entered sea water (21% and 7% degraded), and was transported outside the modelling domain (18%).

According to these results the oceans can play a significant role in global distribution of toxic organochlorines, such as HCHs. These results correspond to that of regional POP transport model including the description of transport with sea currents. As it was mentioned in Chapter 1 current version of the hemispheric model contains a simplified description of air-sea and air-soil gaseous exchange. Therefore, these results are of indicative and preliminary character.

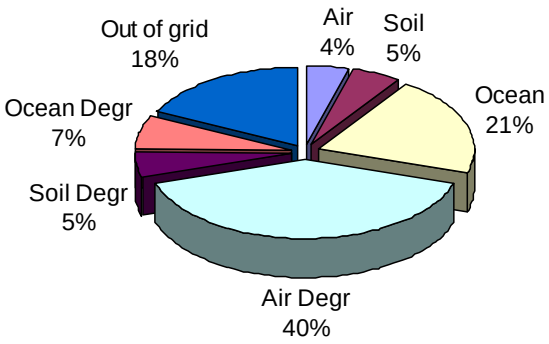


**Figure 3.4.** Mass balance for α-HCH after simulation for 1990

Further, the fact that the amount of pollutant transported outside the grid boundary became essentially smaller than that in regional model (18% for hemispheric model compared with about 60% for regional one) leads to the conclusion that hemispheric modelling scale is more acceptable for organochlorine pesticides such as HCHs.

### 3.1.4 Modelling results for 10-year period

Additional model run covering 10-year period with different emissions was made to test the model description of exchange processes between the atmosphere and underlying surface (soil and sea) from the viewpoint of long-term accumulation in these media. For rough description of the emission reduction, the emission for the first five years of simulation period was taken at the level of 1980, and for the last five years – at the level of 1990. For interpretation of the simulation results the hemispheric grid was divided into five zonal belts which approximately correspond to the five climatic zones (Table 3.5). The belts are equal in size (each of them occupies seven grid cells in the meridional direction) except for the Tropical one (which occupies nine grid cells). Percentage of land and sea in the whole hemispheric grid amounts to 38% for land, 62% for sea.

**Table 3.5.** Division of the hemispheric grid into zonal belts, percentage of land and sea surface in each belt

| | Tropical | Subtropical | Temporal | Boreal | Arctic |
|---|---|---|---|---|---|
| Cell numbers (j) | 1-9 | 10-16 | 17-23 | 24-30 | 31-37 |
| Latitudes | $-1.25^o$-$21.25^o$ | $21.25^o$-$38.75^o$ | $38.75^o$-$56.25^o$ | $56.25^o$-$73.75^o$ | $73.75^o$-$90^o$ |
| Percentage of Land (%) | 24 | 40.5 | 53 | 61.5 | 17.1 |
| Percentage of Sea (%) | 76 | 59.5 | 47 | 38.5 | 82.9 |

Following the applied parameterization of gaseous exchange with underlying surface the major part of $\alpha$-HCH is accumulated in the sea compartment, and essentially less – in the soil compartment. During the first five years of simulation period with emissions of 1980 the accumulation in sea increases from year to year. During the last five years with lower emissions of 1990 it decreases. As seen from diagrams of Figure 3.6 the characteristic time of establishing the quasi-stationarity is much longer for sea than for soil, where pollutant mass practically ceases to increase between the $4^{th}$ and $5^{th}$ years, and very slowly decreases between the $9^{th}$ and $10^{th}$ years. In other words, sea is much more inertial compartment for $\alpha$-HCH than soil (at least with the accepted parameterization). In particular, one can expect that even after full cease of emissions the marine environment will serve as a source of $\alpha$-HCH for some time.

Figure 3.5 shows also the amount of $\alpha$-HCH accumulated in soil and sea in five selected zones (Table 3.5). The accumulation in soil reaches its maximum in the Subtropical zone, while for the sea compartment it is maximum for the Temporal one. The accumulation in soil and sea is conditioned by wet and dry deposition of the gaseous and particle bound phases,

which in turn depend on the emission values and of meteorological parameters. Reduction of α-HCH accumulation in soil and sea is influenced by degradation rate and re-emission from the surface.

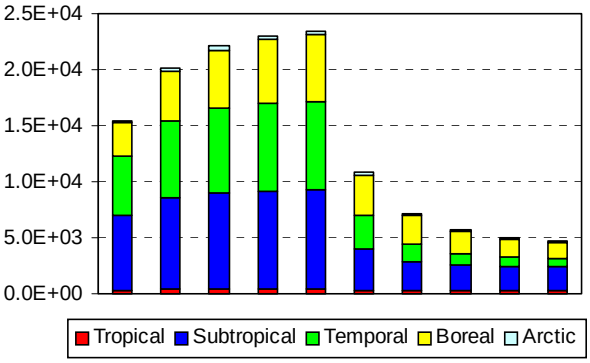


(a) Soil

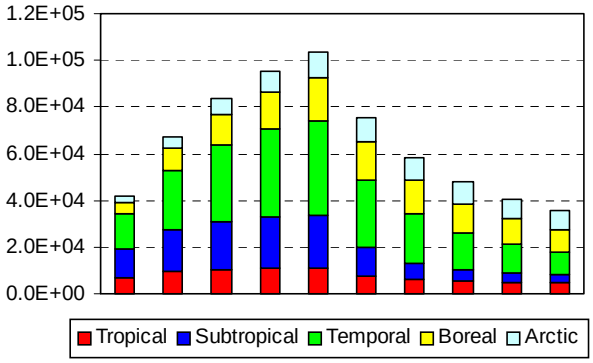


(b) Sea

**Figure 3.5.** Mass in the soil and sea during 10 years of simulations in five zones (tonnes)

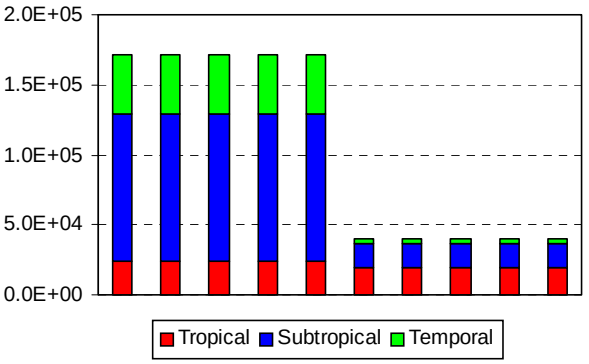


**Figure 3.6.** Annual emissions of α-HCH in five zones for 10 years of simulations, (tonnes)

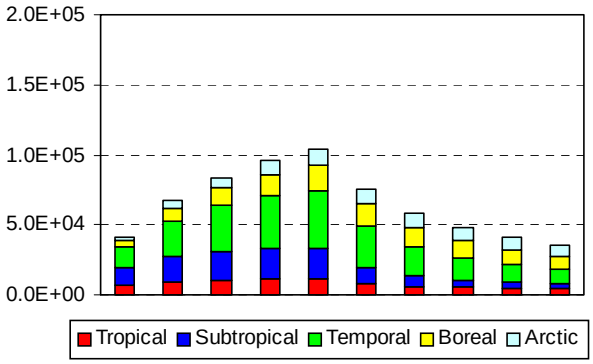


**Figure 3.7.** Total mass accumulated in soil and sea in five zones for 10 years of simulations, (tonnes)

Figure 3.6 shows the emission distribution over the five selected zones and Figure 3.7 – the total mass accumulation including soil and sea. The accumulation is considerable in the Boreal and Arctic zones even if the emissions were small in Boreal zone and absent in Arctic one. These results demonstrate the distribution of α-HCH within the Northern Hemisphere and its accumulation in middle and high latitudes. The latter is most likely connected with the above mentioned cold condensation effect.

Seasonal trends of monthly deposition fluxes for Subtropical and Arctic zones are shown in the Figures 3.8 – 3.11 for 1980 and 1990. These figures represent the gaseous phase exchange flux over the land, wet deposition flux over the land, gaseous phase exchange flux

over the sea, and wet deposition flux over the sea. For demonstrations of these results only two of the five zones were chosen as an example - Arctic and Subtropical.

The correlation of deposition fluxes and variations of emission is pronounced for Subtropical zone, where the emissions are maximum. At the same time in the Arctic zone there is practically no correlation between deposition fluxes and emissions since there is no emission in this zone. Increasing of deposition fluxes in fall and in winter can be connected with the long-range transport of $\alpha$-HCH from emission sources in midlatitudes. Similar results are obtained for dry and wet deposition over seawater in Subtropical zone with the difference that re-emission fluxes from sea surface are less intensive. Re-emission also occurs from the land surface in the Arctic zone mainly in summer months from June to August.

The annual trend of wet deposition flux over land depends on the precipitation amount, air concentration of $\alpha$-HCH, and washout ratio that is the function of temperature. In the Subtropical zone variation of concentrations in the air is mainly connected with variation of emissions. Therefore wet deposition flux correlates with the emission trend (maximum in the first half-year, and near zero in the last half-year). In the Arctic zone such correlation is practically absent.

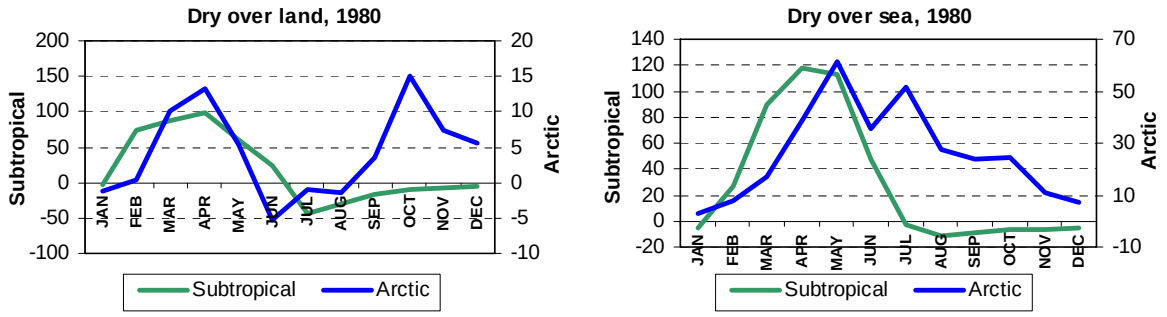


a) b)

**Figure 3.8.** Dry deposition flux of α-HCH over land (a) and over sea (b) in the Subtropical and Arctic zones in 1980, (μg/m$^2$/month)

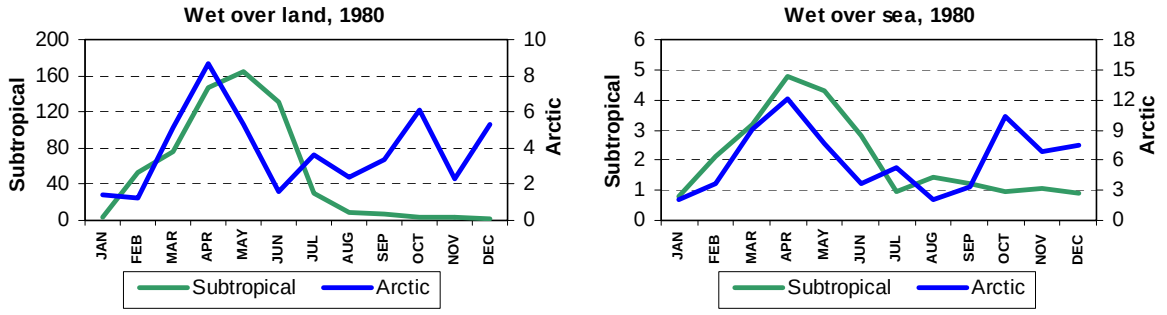


a) b)

**Figure 3.9.** Wet deposition flux of α-HCH over land (a) and over sea (b) in the Subtropical and Arctic zones in 1980, (μg/m$^2$/month)

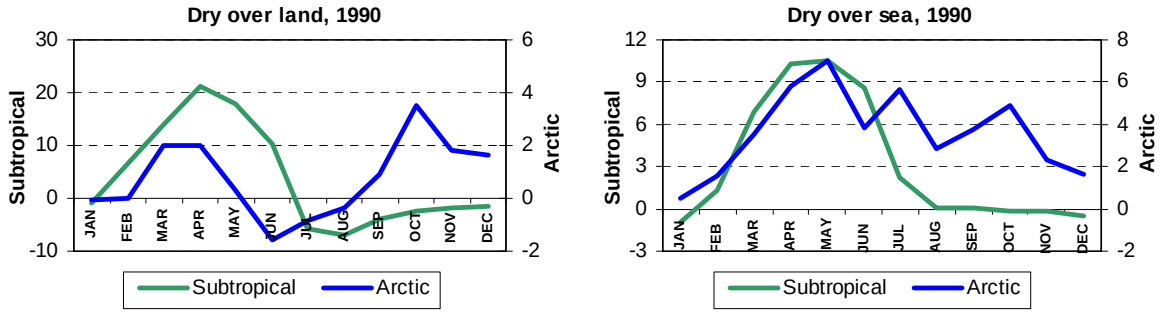


a) b)

**Figure 3.10.** Dry deposition flux of α-HCH over land (a) and over sea (b) in the Subtropical and Arctic zone in 1990, (μg/m$^2$/month)

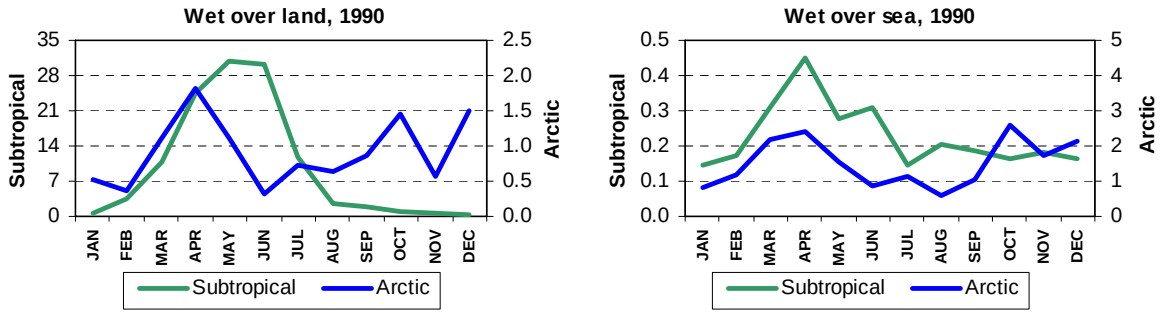


a) b)

**Figure 3.11.** Wet deposition flux of α-HCH over land (a) and over sea (b) in the Subtropical and Arctic zones in 1990, (μg/m$^2$/month)

## 3.2. *Simulation of PCB long-range transport*

The simulation of the long-range transport of polychlorinated biphenyls (PCBs) within the Northern Hemisphere was carried out to compare modelling results of hemispheric and regional models developed at MSC-E [*Pekar et al.*, 1998, 1999]. The latter was used for the simulation of POP long-range transport within European region.

The hemispheric model was run for meteorological situation and emission data for 1990. Meteorological data were obtained using the system of meteorological data supply described in Chapter 2. For the initial conditions PCB concentrations in all model compartments were assumed to be zero. The calculation results were compared with the results of regional model run with the same emission and meteorology data. In both cases the emission of PCBs from European sources only is used.

The modelling domain of the regional model consists of 45x37 grid cells with the resolution of 150x150 km in the horizontal direction and 4 non-uniform vertical layers up to the height of 2100 m. The hemispheric model grid consists of 144x37 grid cells with the resolution 2.5ºx2.5º and 10 non-uniform vertical layers in $\sigma$ co-ordinates. The height of its upper boundary is equal to $\sigma = 0.1$ or approximately 15 km.

### 3.2.1 Physical-chemical properties of PCB-153

For modelling purposes the physical-chemical properties of PCB-153 congener were used for the simulation of the long-range transport of emitted PCB mixture. This set of data for PCB-153 is presented in Table 3.6. These data are taken from the literature and are described in details in report [*Pekar et al.*, 1999].

**Table 3.6.** Physical-chemical properties of PCB-153 used for computations

| Characteristic | Value | Dimensions |
|---|---|---|
| Henry's law constant | $\log H = -\frac{3625}{T} + 13.28$ | Pa $m^3$ $mol^{-1}$ |
| Subcooled liquid pressure | $\log p_L^0 = -\frac{4775}{T} + 12.85$ | Pa |
| Washout ratio for particle bound phase | $W_P = 4\ 10^4$ | - |
| Octanol-water partition coefficient | Log $K_{OW}$ = 3.81 | - |
| Organic C partition coefficient | $K_{OC}$ = 3257 | $m^3\ kg^{-1}$ |
| Degradation rate in air | $K_{Aref} = 3.5\ 10^{-8}$ | $s^{-1}$ |
| Degradation rate in soil | $K_{Sref} = 8.79\ 10^{-8}$ | $s^{-1}$ |
| Degradation rate in sea | $K_{Wref} = 2.2\ 10^{-8}$ | $s^{-1}$ |
| Molecular diffusivity in air | $5.0\ 10^{-6}$ | $m^{-2}\ s^{-1}$ |
| Molecular diffusivity in water | $5.0\ 10^{-10}$ | $m^{-2}\ s^{-1}$ |

### 3.2.2 Emission of PCBs

The simulation was performed for European emissions of PCBs in 1990 [*Berdowsky et al.*, 1997]. Figure 3.12 represents the spatial distribution of annual PCB emissions for 1990. It is assumed that PCB emissions have no seasonal variation and are distributed uniformly throughout the year. The total emission amounts to 112 tonnes for the whole grid.

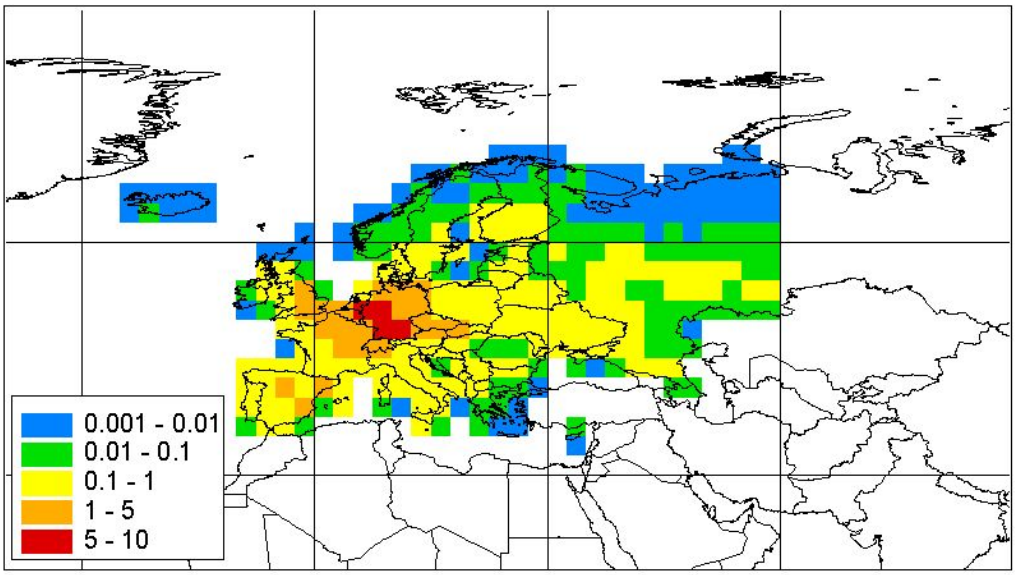


**Figure 3.12.** European emission of PCBs for 1990, (t/cell/yr)

### 3.2.3 Comparison of modelling results of regional and hemispheric models

As it was mentioned above the simulation of PCB long-range transport was performed using regional and hemispheric models to compare their results. Two models were run with the same emission data, for the same year 1990 and with the same physical-chemical properties of the pollutant. The corresponding mass balances for 1990 are shown on the Figure 3.13.

In the regional model about 70% of total annual PCB emission is transported outside the computational grid. The deposition within the borders of the grid over the land reaches 15% of total PCB emission and over sea - 10%. For the hemispheric model the transport outside the grid is about 15%, and the deposition over the land reaches 35% and over the sea – 25%.

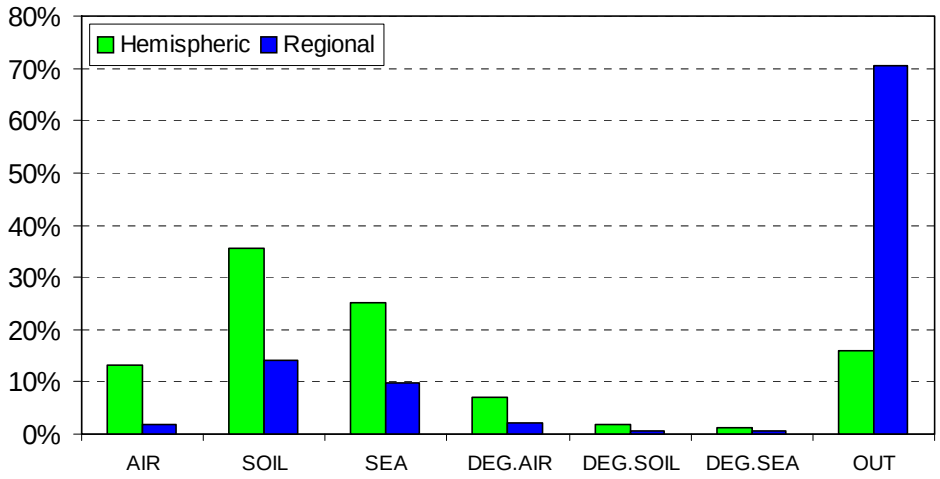


**Figure 3.13.** Mass balance for PCB after simulations of 1990 using regional and hemispheric models, where:

AIR, SOIL, SEA - PCB mass in air, soil, sea compartments;
DEG.AIR, DEG.SOIL, DEG.SEA - PCB mass degraded in air, soil, sea compartments;
OUT - PCB mass transported out of the model grid

As it follows from the figure the most pronounced differences between two models are connected with the amount of the pollutant transported outside the computational grid. Comparably high difference in the air content is partly a consequence of extension of model domain in vertical direction. The rest of the parameters are changed proportionally to the amount of the pollutant remained within the modelling domain. On the whole, the comparison of PCB mass balances obtained using these two models demonstrates reasonable agreement of their results. Besides, the results of PCB regional modelling performed in 2000 showed that calculated concentrations in all the media were somewhat lower than observations. This most likely connected with the influence of emission sources,

which was not taken into account. Therefore regional model can be used in combination with hemispheric one, i. e. on the basis of hemispheric model results it is possible to set up background concentrations and boundary conditions.

Spatial distribution of mean annual PCB air concentrations and accumulated total depositions is shown on the following four Figures 3.14-3.17. In general both models provides similar levels of concentrations and depositions of PCB in 1990 in European region. Some differences can be however noted in the distance of pollutant transport. Namely, for the hemispheric model, which has larger modelling domain in horizontal and vertical directions the transport, distance is longer. On the whole, the spatial distributions obtained with these two models are again in the reasonable agreement with each other.

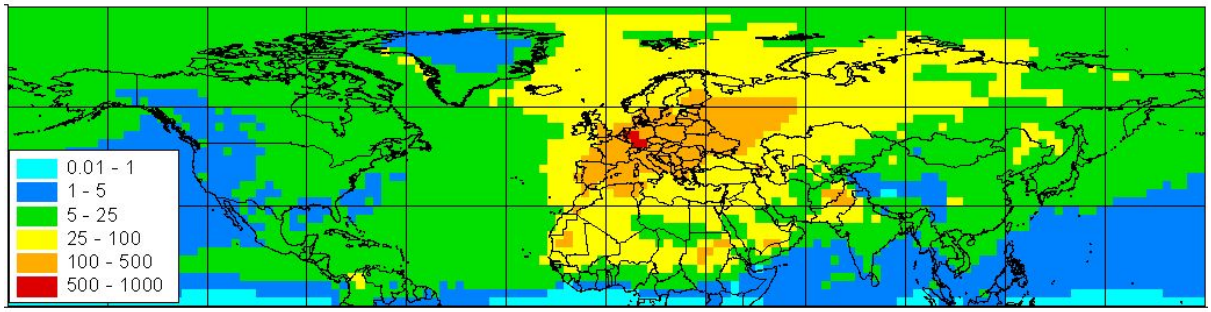


**Figure 3.14.** Mean annual air concentration of PCB, pg $m^{-3}$
(computations were made with the hemispheric model)

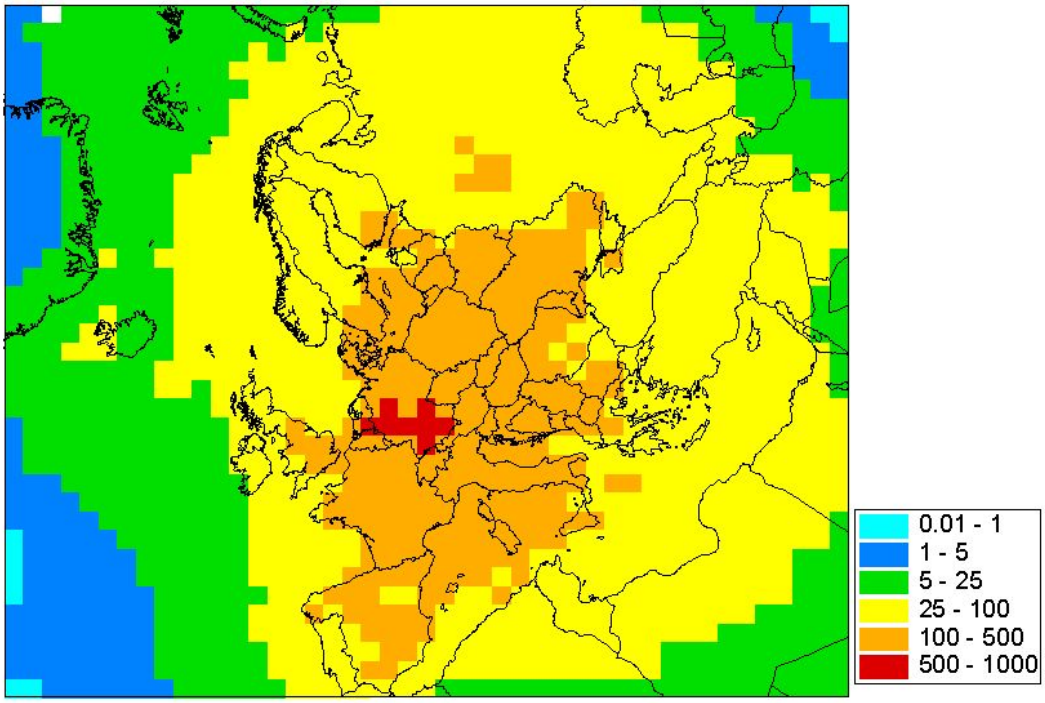


**Figure 3.15.** Mean annual air concentration of PCB, pg $m^{-3}$
(computations were made with the regional model)

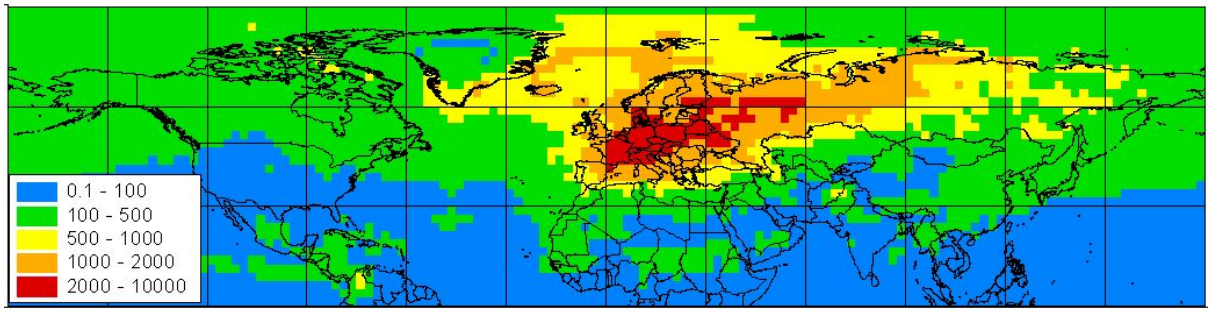


**Figure 3.16.** Total depositions of PCB over the year, ng/m$^2$/yr (computations were made with the hemispheric model)

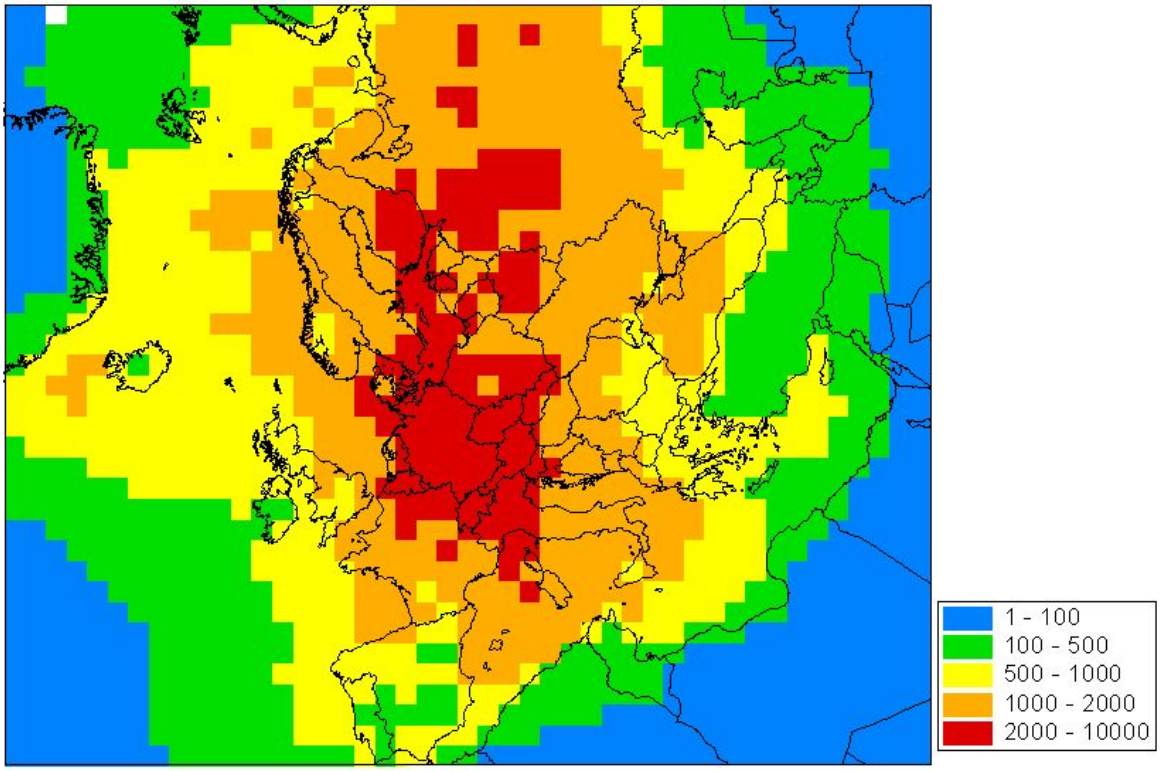


**Figure 3.17.** Total deposition of PCB over the year, ng/m$^2$/yr (computations were made with the regional model)

## *Conclusions*

- Following the recommendations of the Steering Body to EMEP and the Geneva workshop [*WMO/GAW No.136,* 2000] MSC-E has started the development of HM and POP multi-compartment transport models on the hemispheric scale.

- For preparation of meteorological information for modelling within the Northern Hemisphere a special System of Diagnosis of lower Atmosphere (SDA) was developed. This system provides a set of meteorological data according to the requirements of hemispheric and regional multi-compartment models being developed at EMEP/MSC-E.

- The preliminary results of POP hemispheric modelling are in a reasonable agreement with those obtained by MSC-E regional model both in mass balance and in spatial distribution of air concentrations and depositions.

- The model experiments with the first version of the hemispheric model carried out on the example of some POPs (PCBs, $\alpha$-HCH) showed that some effects known in the literature, such as cold condensation, are reproduced by the model.

- At further stage the hemispheric multi-compartment model is to be improved with the description of the processes of air/vegetation exchange and the transport by sea currents. It is planned also to modify this model for mercury modelling.

- Hemispheric modelling can be applied for supplying regional models dealing with volatile and semi-volatile compounds with appropriate boundary conditions and initial information. This consequently can result in improvement of agreement between measurements and model computations for the EMEP domain.

- The hemispheric model will be used for the assessment of the long-range transport of HMs and POPs in the Northern Hemisphere with specific emphasis to the Arctic region.

# *References*


Berdowski J.J.M., Baas J., Bloos J.P.J., Visschedijk A.J.H. and P.Y.J.Zandveld [1997] The European emission inventory of heavy metals and persistent organic pollutants for 1990. TNO Institute of Environment Science, Energy Research and Process Innovation, UBA-FB report 104 02 672/03, Apeldoorn, pp.239.

Bizova N.L. [1987] On reproduction of vertical profiles of the atmospheric boundary layer characteristics using limited meteorological information. Meteorology and Hydrology, 11.

Frolov A., Rubinstein K., Rosinkina I., Vajnik , Kiktev D., Astachova E. and J.Alferov [1994] A System of diagnosis of lower atmosphere for of transboundary air pollutant transport. EMEP/MSC-E and RHMC report 1/94.

Frolov A., Vaznik A., Astahova E., Alferov J., Kiktev D., Rosinkina I. and K.Rubinstein [1997] A System of diagnosis of lower atmosphere for monitoring transboundary pollutant transport. *Meteorology and Hydrology*, N4, pp.5-15.

Frolov A., Vaznik A., Astahova E., Alferov J., Kiktev D., Rosinkina I. and K.Rubinstein [1997] A System of diagnosis of lower atmosphere for monitoring transboundary pollutant transport. The main algorithms. *Meteorology and Hydrology*, N5, pp.5-13.

Frolov A., Vaznik A., Astahova E., Alferov J., Kiktev D., Rosinkina I. and K.Rubinstein [1997] A System of diagnosis of lower atmosphere for monitoring transboundary pollutant transport: Precipitation and clouds. *Meteorology and Hydrology*,N6, pp.5-15.

Hinckley D., Bidleman T. and C.Rice [1991] Atmospheric Organochlorine Pollutants and Air-Sea Exchange of Hexachlorocyclohexane in the Bering and Chukchi Seas, Jornal og Geophysical Research, v.96, No.C4, pp.7201-7213.

Iwata H., Tanabe S., Sakai N. and R.Tatsukawa [1993] Distribution of Persistent Organochlorines in the Oceanic Air and Surface Seawater and the Role of Ocean on Their Global Transport and Fate, *Environ. Sci. Technol*., 27, pp.1080-1098.

Jacobs C.M.J. and W.A.J. van Pul [1996] Long-range atmospheric transport of persistent organic pollutants, I: Description of surface-atmosphere exchange modules and implementation in EUROS. National Institute of Public Health and the Environment, Bilthoven, The Netherlands. Report No.722401013.

Junge C.E. [1977] Basic considerations about trace constituent in the atmosphere is related to the fate of global pollutant. In: Fate of pollutants in the air and water environment. Part I, I.H. Suffer (ed.) (Advanced in Environ. Sci. Technol., v.8), Wiley-Interscience, New York.

Kurbatkin G.P., Degtarev A.I. and A.V.Frolov [1994] Spectral model of the atmosphere, initialization and database for numeric weather forecasts. – Sn.-P., Hydrometeoizdat, p.184.

Li Y.F., Scholtz M.T. and B.J.van Heyst [1999] Global gridded emission inventories of $\alpha$-hexachlorocyclohexane, J. *Geophys. Res*. In press.

Pacyna J.M. et al. [1999] Technical Report. Appendix 1to Executive Final Summary Report. Environmental Cycling of Selected Persistent Organic Pollutants (POPs) in the Baltic Region (Popcycling-Baltic project). Contract No. ENV4-CT96-0214. CD-ROM.

Pankow J.F. [1987] Review and comparative analysis of the theories on partitioning between the gas and aerosol particulate phase in the atmosphere. *Atmos. Environ*., 21, pp.2275-2283.

Pekar M. [1996] Regional model LPMOD and ASIMD. Algorithms, parameterization and results of application to Pb and Cd in Europe scale for 1990. MSC-E Report 9/96, September.

Pekar M., Gusev A., Pavlova N., Strukov B., Erdman L., Ilyin I, and S.Dutchak [1998] Long-range transport of selected POPs. Development of transport models for lindane, polychlorinated biphenyls, benzo(a)pyrene. EMEP/MSC-E Report 2/98, Part I.

Pekar M., Pavlova N., Gusev A., Shatalov V., Vulikh N., Ioannisian D., Dutchak S., Berg T. and A.-G.Hjellbrekke [1999] Long-range transport of selected persistent organic pollutants. EMEP/MSC-E and CCC Report 2/99, July 1999.

Reynolds R.W. and T.M.Smith [1994] Improved global sea surface temperature analyses using optimum interpolation. J. *Climate*, 7, pp.929-948.

Rubinstein K., Frolov A., Vaznik A., Astachova E., Rosinkina I., Kiktev D. and J.Alferov [1997] Diagnostic System of Atmosphere Lower-Layer for Pollution Transfer Modelling. Revista. International de Contaminational. Ambienal. 13 (1), pp.23-34.

Rubinstein K. and D.Kiktev [1998] Comparison System of the Atmospheric Lower-Layer Diagnostic System(SDA) for Pollution Transfer Modeling of MSC - East(Moscow) and MSC - West(Oslo). Proceeding of International Conference of Air Pollution Modeling and Simulation. Paris, 26-29 October 1998.

Rudolf B. [1993] Management and Analysis of Precipitation data on a Routine Basis. Proceedings Int. Symp. on Precipitation. (Ed. B.Sevruk and M.Lapin), ETH Zuerich, v.1, pp.69-76.

Samarsky A.A. [1977] Theory of finite-difference schemes. Moscow, «Nauka», p.656.

Sehmel G.A. [1980] Particle and gas dry deposition: a review. *Atmospheric Environment*, 14, pp.983-1011.

Smolarkiewicz P.K. (1983) A simple positive definite advection scheme with small implicit diffusion. Monthly Weather Review, v.111, pp.479-486.

Strand A. and O.Hov (1996) A model strategy for the simulation of chlorinated hydrocarbon distributions in the global environment. *Water, Air, and Soil Pollution*, v.86, pp.283-316.

Wania F. and D.Mackay [1995] A global distribution model for persistent organic chemicals. *The Science of the Total Environment*, v.160/161

WMO/GAW [2000] Report and proceedings of the workshop on modelling of atmospheric transport and deposition of persistent organic pollutants and heavy metals (Geneva, Switzerland, 16-19 November, 1999). WMO/TD No.1008.